EXPANSION OF NUMERICAL MODEL CSHORE TO PREDICT EROSION AND OVERWASH OF WOODED DUNES

BY

BERNA AYAT AND NOBUHISA KOBAYASHI

RESEARCH REPORT NO. CACR-13-07
DECEMBER 2013

Sponsored by
U. S. Army Corps of Engineers

CENTER FOR APPLIED COASTAL RESEARCH

Ocean Engineering Laboratory
University of Delaware
Newark, Delaware 19716

ACKNOWLEDGEMENT

This study has been supported partly by the U.S. Army Corps of Engineers under Contract No. W911XK-13-P-0065.

The first author was supported by the Scientific and Technological Research Council of Turkey during her one-year stay at the Center for Applied Coastal Research, University of Delaware. This report is based on the paper entitled, "Stem Density and Toppling Effects on Wooded Dune Erosion and Overwash," which has been accepted for publication in *Journal of Waterway, Port, Coastal and Ocean Engineering*.

Contents

Expansion of Numerical Model CSHORE to Predict Erosion and Overwash of Wooded Dunes

Berna Ayat[1], and Nobuhisa Kobayashi[2]

Abstract: Interactions among waves, sand dunes and woody plants are investigated to quantify the role of woody plants in dune erosion and overwash. A cross-shore numerical model is expanded to include the drag force acting on wooden dowels (idealized stems). The hydrodynamic variables modified by the dowels are used to predict bed load and suspended sand transport rates. The expanded model is compared with previous five tests. The drag coefficient is calibrated to obtain similar agreement for the dunes with and without the dowels. Four tests were conducted to examine the placement density and toppling of the dowels. The effectiveness of the dowels in reducing dune erosion and overwash decreased significantly with the density decrease and dowel toppling. The reduced effectiveness is reproduced by the expanded model with the calibrated drag coefficient. However, a simple toppling criterion needs to be adjusted for each test for the reproduction of the observed landward progression of dowel toppling during the dune profile evolution. Field data will be required to improve the dowel model for real woody plants.

1. Introduction

Grass and woody plants have been used for dune stabilization against windblown sand transport but their effects on dune erosion and overwash have not been investigated comprehensively. Gralher et al. (2012) conducted five tests in a laboratory experiment to examine the effects of woody plants on erosion and overwash of high and low dunes where cylindrical dowels were used to represent woody plants. The dowels placed on the foreslope and backslope of the high

[1] Research Associate, Department of Civil Engineering, Yildiz Technical University, Esenler, Istanbul 34220, Turkey.
[2] Professor and Director, Center for Applied Coastal Research, University of Delaware, Newark, DE 19716.

dune were effective in reducing dune erosion and delaying wave overtopping and overwash. The dowels were observed to retard wave uprush on the foreslope but increased offshore sand transport from the eroded dune (Kobayashi et al. 2013). The offshore sand transport and deposition reduced the water depth in the surf zone and may have slowed the subsequent dune erosion and overwash. The complicated interactions among the waves, dowels and sand dunes observed in the experiment may be interesting but the experiment was limited to the specific diameter, height, spacing, alignment and burial depth of rigid wooden dowels without toppling.

The dowel density N defined as the number of dowels per unit horizontal area is given by $N = 1/S^2$ for the uniform spacing S used in the previous experiment. The dowel effect on dune erosion and overwash is expected to become negligible if the dowel density becomes sufficiently small. The pilings of elevated buildings are normally spaced widely to allow the passage of waves under the buildings during storms (e.g., Edge et al. 2010). The field data in southern Thailand by Horstman et al. (2012) indicated the increase of wave attenuiation in mangrove forests with the vegetation density. Moreover, a dowel can be toppled by the wave force when erosion reduces its burial depth sufficiently. The progressive toppling of dowels will diminish their effectiveness in reducing dune erosion and overwash. Matsutomi et al. (2012) analyzed the lodging, uprooting and breaking of coastal pine trees caused by the 2011 Tohoku Earthquake Tsunami and the role of a belt of the trees in reducing the tsunami energy and force. Additional four tests were conducted in this study to quantify the dowel density and toppling effects.

A number of parameters are required to characterize woody plants. A numerical model is needed to synthesize all test results for field applications. The cross-shore model CSHORE based on the assumption of alongshore uniformity has been compared with field and laboratory data on

dune erosion and overwash (Kobayashi et al. 2010; Figlus et al. 2011; Kobayashi and Jung 2012). In the following, CSHORE is expanded to include the drag force acting on the dowels. The expanded model is compared with the previous five tests and the drag coefficient is calibrated. The calibrated model is used to devise additional four tests with noticeable differences caused by the dowel density and toppling.

2. Numerical Model CSHORE

The cross-shore model CSHORE is expanded to wooded dunes as shown in Fig. 1. The vertical coordinate z is positive upward with $z = 0$ at the still water level (SWL). The origin of the onshore coordinate x is chosen at the offshore location of the irregular wave measurement. The still water shoreline is located at $x = x_{SWL}$. The instantaneous water depth h is given by $h = (\eta - z_b)$ where $\eta =$ free surface elevation above SWL and $z_b =$ local bottom elevation which is negative below SWL. The instantaneous depth-averaged velocity U is positive onshore. The vegetation is simply represented by a number of rigid dowels or piles without branches and leaves and can be located in the wet zone $(x < x_{SWL})$ and the wet and dry zone $(x > x_{SWL})$ during the beach and dune profile evolution. The fraction of the bottom area occupied by the dowels is assumed to be small.

The instantaneous drag force τ_d' acting on the dowels per unit horizontal area may be expressed as

$$\tau_d' = \frac{1}{2}\rho C_D b N h_* |U| U \tag{1}$$

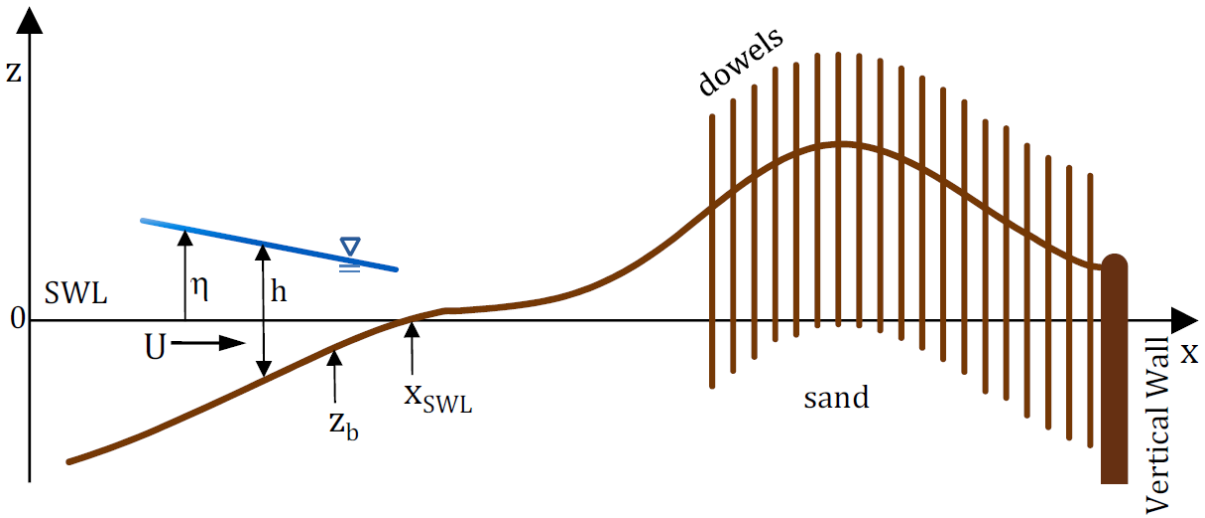

Figure 1. Definition sketch for wave overwash of dune with dowels

where ρ = fluid density; C_D = drag coefficient; b = width of each dowel normal to the horizontal velocity U ; N = number of dowels per unit horizontal area; and h_* = submerged height of the dowel which equals the smaller value of the instantaneous water depth h and the dowel height d above the sand surface located at $z = z_b$. The vegetation characteristics expressed by b, N, and d are allowed to vary spatially where $b = 0$, $N = 0$ and $d = 0$ in the zone of no dowel. The drag coefficient is assumed to be constant and calibrated in the range of C_D = 1 – 2 on the basis of available wave force data for a single pile presented by Tørum, (1989) who measured wave forces in the surface zone affected by the free surface oscillation. The calibrated value of C_D = 1.9 used in the following computations is explained later. The calibration is necessary for lack of data for piles in the swash zone.

In the wet zone, CSHORE computes the cross-shore variations of the mean and standard deviation of η and U using the time-averaged continuity, momentum, and energy equations based on linear wave theory and the Gaussian probability distribution of η and U . The equivalency of the time and probabilistic averaging is assumed and indicated by the overbar. The instantaneous height h_* in Eq. (1) is approximated by the smaller value $\overline{h_*}$ of the mean depth $\overline{h}$ and d to be consistent with the use of linear wave theory. The mean depth $\overline{h}$ is given by $\overline{h} = \left(\overline{\eta} - z_b\right)$ with $\overline{\eta}$ = mean water level. The time-averaged drag force τ_d combined with the time-averaged bottom shear stress τ_b in the time-averaged momentum equation may be expressed as

$$\tau_d + \tau_b = \frac{1}{2}\rho f_{bd}\overline{|U|U} \quad ; \quad f_{bd} = f_b + C_D b N \overline{h_*} \tag{2}$$

where f_b = bottom friction factor of the order of 0.01 for sand beaches; and f_{bd} = equivalent bottom friction factor which varies spatially but is independent of time. The increased flow resistance due to the vegetation is thus included in the equation of τ_b in CSHORE using f_{bd} in place of f_b. The energy dissipation rate D_f due to bottom friction in the time-averaged energy equation is also expressed using f_{bd} in place of f_b to account for the increased energy dissipation and sand suspension in the dowel zone.

In the wet and dry zone, CSHORE employs the time-averaged continuity and momentum equations derived from the nonlinear shallow-water wave equations. The probabilistic averaging of $h_* |U| U$ in Eq. (1) is necessary to account for the asymmetry of wave uprush and downrush in the swash zone. The probability density function $f(h)$ of the instantaneous water depth h is assumed to be exponential

$$f(h) = \frac{P_w^2}{\overline{h}} \exp\left(-P_w \frac{h}{\overline{h}} \right) \quad \text{for} \quad h > 0 \tag{3}$$

where P_w = wet probability for $h > 0$; and $\overline{h}$ = mean water depth for the wet duration. The overbar indicates averaging for the wet duration only. The cross-shore velocity U in the wet and dry zone is assumed to be expressed as

$$U = \alpha \sqrt{gh} + U_s \tag{4}$$

where α = empirical parameter of the order of 2; g = gravitational acceleration; and U_s = steady velocity included to account for offshore return flow on the foreslope of the dune and the downward velocity increase on the backslope. The probabilistic averaging of Eq. (1) in the wet and dry zone is based on

$$\overline{h_* |U| U} = \int_0^d h |U| U \, f(h) dh + \int_d^\infty d \, |U| U f(h) dh \tag{5}$$

where $h_* = h$ for $h < d$ and $h_* = d$ for $h > d$. Eqs. (3) and (4) are substituted into Eq. (5) to integrate Eq. (5) analytically after lengthy algebra.

The time-averaged drag force τ_d in the wet and dry zone can be shown to be expressed as

$$\tau_d = \frac{\rho C_D b N g \left(\alpha \bar{h}\right)^2}{2 P_w} G_d(r, \xi) \; ; \; r = \frac{U_s \sqrt{P_w}}{\alpha \sqrt{g \bar{h}}} \; ; \; \xi = \frac{d P_w}{\bar{h}} \tag{6}$$

where the dimensionless function G_d depends on the dimensionless parameters r and ξ. The velocity U_s can be negative (offshore) or positive (onshore). The vegetation height d is positive or zero. For the case of $r \ge 0 \left(U_s \ge 0\right)$, G_d is given by

$$G_d = 2 - (\xi + 2) e^{-\xi} + r \left[\sqrt{\pi} \xi - 3 \sqrt{\xi} \, e^{-\xi} + \sqrt{\pi} \left(\frac{3}{2} - \xi \right) erf\left(\sqrt{\xi}\right) \right] + r^2 \left(1 - e^{-\xi}\right) \tag{7}$$

where *erf* is the error function. For the case of $r < 0$ and $\xi \le r^2$, G_d is expressed as

$$G_d = 2\xi \exp\left(-r^2\right) - 2 - r^2 + \sqrt{\pi} r \left[\left(\xi - \frac{3}{2} \right) erf\left(\sqrt{\xi}\right) + 2\xi \, erf(r) + \xi \right] + \left(\xi + 2 + r^2 + 3r\sqrt{\xi} \right) e^{-\xi} \tag{8}$$

For the case of $r < 0$ and $\xi > r^2$, G_d is given by

$$G_d = 4 \exp\left(-r^2\right) - r^2 - 2 + 3\sqrt{\pi} r \, erf(r) + \sqrt{\pi} r \left[\xi + \left(\frac{3}{2} - \xi \right) erf\left(\sqrt{\xi}\right) \right] - \left(\xi + 2 + r^2 + 3r\sqrt{\xi} \right) e^{-\xi} \tag{9}$$

The drag force τ_d given by Eq. (6) is added to the bottom shear stress τ_b in the time-averaged momentum equation to compute the cross-shore variation of the mean depth $\bar{h}$ in the same way as in CSHORE with no dowel. The equations of the standard deviation σ_η of the free surface

elevation η, the wet probability P_w, and the mean $\overline{U}$ and standard deviation σ_U of the cross-shore velocity U are the same as those in CSHORE with no dowel (Kobayashi et al., 2010).

After the computation of $\overline{h} = \left(\overline{\eta} - z_b\right), \sigma_\eta, P_w, \overline{U}$ and σ_U for given z_b, the time-averaged bed load and suspended sediment transport rates are computed using the formulas given by Kobayashi et al. (2010) and modified slightly by Figlus et al. (2011). The sediment transport rates are influenced by the dowels through the hydrodynamic variables which are affected by the drag force τ_d and the energy dissipation rate D_f due to the drag force and bottom shear stress. The buried parts (idealized roots) of the dowels in Fig. 1 may reinforce the sand against scarping of the steep foreslope of the dune (Kobayashi et al., 2013) but the sand reinforcement effect is hard to quantify and may be neglected in this first attempt to elucidate the interactions among the waves, dowels and sand. The computed sediment transport rates and the continuity equation of bottom sediment are used to compute the bottom elevation z_b at the next time level. This time-marching computation starting from time $t = 0$ is repeated for the duration of each test in the following comparisons. The input parameters for CSHORE are kept the same as those used by Figlus et al. (2012) who calibrated CSHORE extensively.

3. Comparisons with High and Low Dune Tests

The expanded model is compared with the experiment conducted by Gralher et al. (2012) in the wave flume which is 30 m long, 1.15 m wide and 1.5 m high. The sand beach in the flume consisted of well-sorted fine sand with a median diameter of 0.18 mm. The measured specific gravity, porosity and fall velocity were 2.6, 0.4 and 2.0 cm/s, respectively. The piston-type wave maker in a 1-m depth generated a 400-s burst of irregular waves corresponding to a TMA

spectrum. The spectral significant wave height and peak period were approximately 19 cm and 2.6 s, respectively. This experiment did not scale specific prototype conditions but the fine sand in the experiment could be regarded as coarse sand at prototype scale. Eight capacitance wave gauges were used to measure the cross-shore and temporal variations of the free surface elevation where the most seaward wave gauge was located well outside the surf zone and its location is taken as $x = 0$ in Fig. 1. Three acoustic Doppler velocimeters were used to measure fluid velocities in the surf zone. The horizontal locations of the free surface elevation and velocity measurements are shown later in conjunction with the comparison of the measured and computed values. A laser line scanner mounted on a motorized cart and an array of three submerged ultrasonic transducers were used to measure the subaerial (after lowering the water level) and submerged portions of the bed, respectively. The measured bottom elevations were averaged alongshore to obtain the beach and dune profile as a function of x at time t with $t = 0$ at the beginning of each test. A vertical wall was located at x = 19.9 m in Fig. 1 and its crest elevation was 6 cm above SWL. Water and sand transported over the vertical wall during each 400-s run were collected in a basin to measure the water overtopping rate and sand overwash rate averaged over the 400-s run.

Three high (H) dune tests and two low (L) dune tests were conducted in sequence. The initial profile of the high dune was the same for the three tests where the dune crest elevation was 21 cm above SWL and the foreslope and backslope of the dune were 1/2 and 1/3, respectively, where the slope was defined as the ratio between the vertical and horizontal distances. The high dune of the first test was bare (B) with no dowel. This HB test was terminated after 6 runs when the dune crest was lowered to the elevation of the wall crest.

Cylindrical wooden dowels were used to represent woody plants. The diameter and

length of each dowel were 0.9 cm and 30 cm, respectively. Each dowel was placed vertically with a burial depth of 20 cm. The burial depth of each dowel was checked after each run and adjusted to 20 cm at the beginning of each run to avoid toppling. The horizontal spacing S among the dowels was 4 cm. This experiment was limited to b = 0.9 cm, d = 10 cm (d/b = 11), and $N = 1/S^2$ with S = 4 cm (S/b = 4.4) in Eq. (1).

Narrow (N) and wide (W) dowel zones were examined in the second and third tests. The narrow dowel zone was located between x = 19.5 m and 19.9 m on the backslope. The wide dowel zone between x = 19.1 m and 19.9 m covered the foreslope and backslope. HN test was terminated after 6 runs because the narrow dowel did not reduce dune erosion and overwash in comparison to HB test. The wide dowel zone reduced the foreslope erosion and scarping significantly because the dowels reduced wave uprush velocities. HW test was terminated after 28 runs due to alongshore profile variability. The final profile of HW test was smoothed and made uniform alongshore to create the initial profile of the low dune tests LB and LW. LB test was terminated after 3 runs due to intense wave overtopping and overwash. The wide dowel zone for LW test reduced wave uprush and overtopping. LW test was continued for 20 runs.

Comparisons are made for the measured and computed cross-shore variations of $\overline{\eta}$, σ_η, $\overline{U}$, σ_U, and P_w for each run of HB, HN, HW, LB and LW tests where the run number is affixed to the test name to indicate the profile evolution in each test. Fig. 2 shows the comparisons for HW1 (first) and HW28 (last) runs as examples. The measured values of the spectral significant wave height $H_{mo} = 4\sigma_\eta$, the spectral peak period T_p, and the mean water level $\overline{\eta}$ (wave setdown of about 2 mm) at $x = 0$ are specified as the boundary conditions for each run. The computed bottom elevation z_b is shown in the top panel to indicate the mean depth

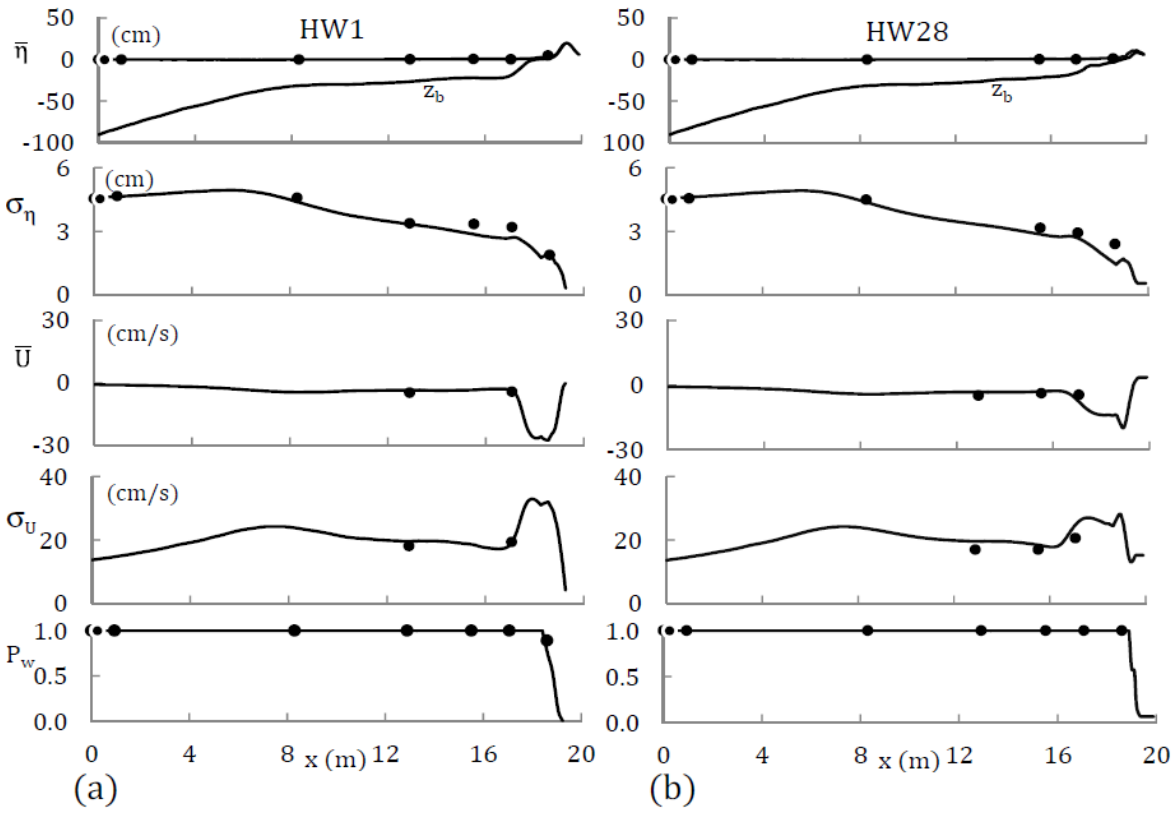

Figure 2. Measured (circles) and computed (solid lines) mean and standard deviation of η and U together with wet probability P_w for (a) HW1 and (b) HW28 runs.

$\overline{h} = \left(\overline{\eta} - z_b\right)$. The measured bottom elevation seaward of x = 16 m did not change much probably because a number of preliminary runs were conducted to optimize the experimental setup. The mean water level is almost the same as SWL except in very shallow water. The second panel for σ_η indicates the shoaling and breaking of irregular waves and the landward decrease of the swash motion. The cross-shore velocity measured at an elevation of 1/3 of the local water depth above the bottom is compared with the computed depth-averaged velocity U in the third and fourth panel. The return current velocity $\overline{U}$ is negative (offshore) and approximately −5 cm/s except in very shallow water where the computed mean velocity $\overline{U}$ is strongly offshore on the berm and foreslope of the dune and weakly onshore on the backslope due to wave overtopping. The velocity standard deviation representing the oscillatory wave velocity remains almost the same except in very shallow water where the computed value of σ_U becomes large on the berm. The wet probability P_w is unity in the wet zone seaward of the still water shoreline and decreases rapidly in the wet and dry zone. The measured value of P_w at the most landward wave gauge located at x = 18.6 m is obtained as the ratio between the wet and total durations. It is noted that the values of $\overline{\eta}$, σ_η, $\overline{U}$, and σ_U in the wet and dry zone are based on the wet duration only. CSHORE predicts these hydrodynamic variables within errors of about 20%.

The number of 400-s runs for HB, HN and HW tests were 6, 6 and 28, respectively. Fig. 3 compares the measured and computed dune profiles at the end of three runs in the zone of x = 16 – 19.9 m of noticeable profile changes in front of the vertical wall. The dowel zone is indicated in Fig. 3 and subsequent figures. The profile evolution from the initial profile is

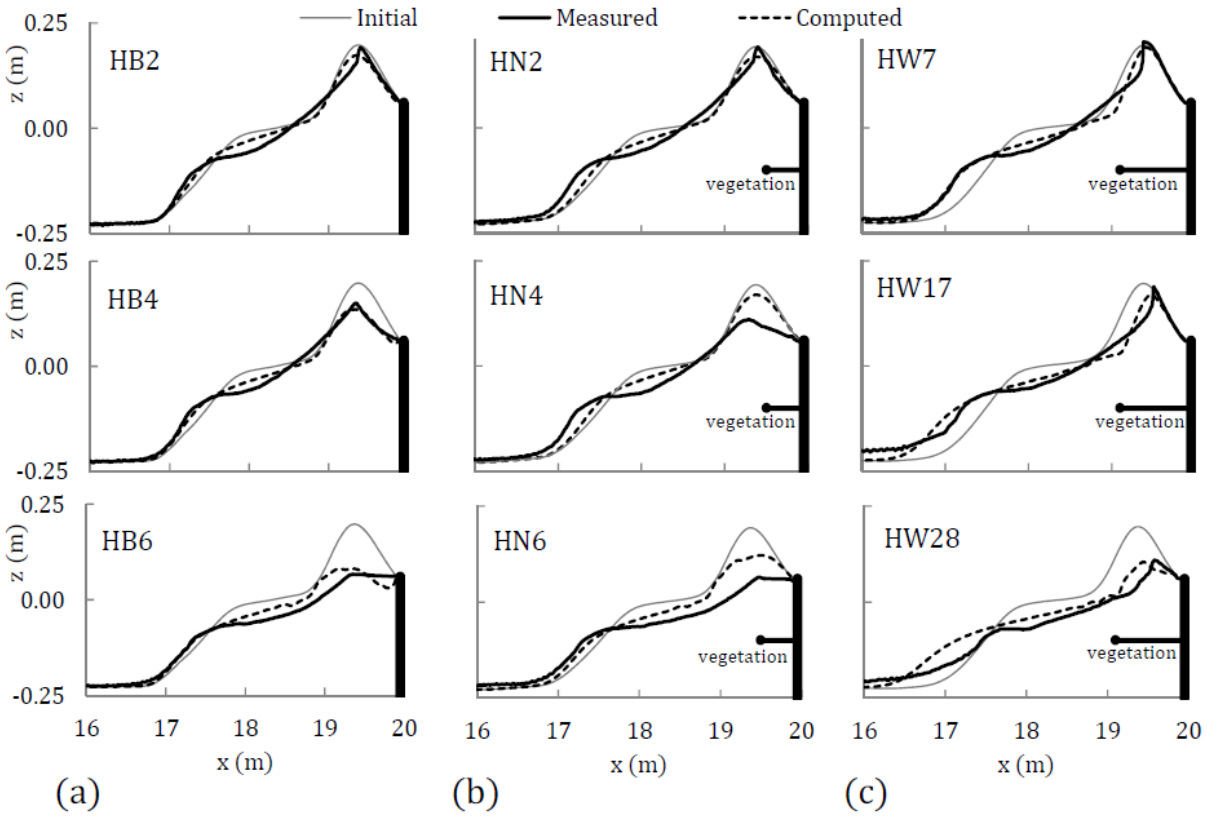

Figure 3. Measured and computed dunr profiles at the end of three runs for (a) HB, (b) HN and (c) HW tests.

predicted well for HB test with no dowel where HB2, HB4 and HB6 correspond to the second, fourth and last runs, respectively. For HN test with the dowel zone x = 19.5 – 19.9 m, the dune crest lowering is underpredicted. For HW test with the dowel zone x = 19.1 - 19.9 m, the dune crest lowering during the 28 runs is predicted well but the steep scarped profile of the foreslope is not predicted adequately for HW7 and HW17.

The measured wave overtopping rate q_o and overwash rate q_{bs} are the average rates during each 400-s run and plotted at time t corresponding to the middle of each run. The computed values of q_o and $q_{bs} = (q_b + q_s)$ are also averaged during each run where q_b and q_s are the computed bed load and suspended sediment transport rates at x = 19.9 m. The measured and computed temporal variations of q_o and q_{bs} are compared in Fig. 4. For HB test, q_o and q_{bs} are overpredicted at the beginning of the test with no or little wave overtopping and overwash. For HN test, q_o and q_{bs} are underpredicted at the end of the test because of the underprediction of the dune crest lowering in Fig. 3. For HW test, wave overtopping and overwash did not occur until HW21 (t = 8,000 – 8,400 s) and the measured values of q_o and q_{bs} were relatively small even at the end of the test. These measured trends are predicted well partly because the drag coefficient C_D = 1.9 in Eq. (1) is calibrated for HW test which is the most sensitive to C_D. The agreement for HN test could be improved by reducing C_D but C_D is kept the same to indicate the limitation of the adopted dowel model.

For the low dune tests, no berm was present from the beginning of LB and LW tests. The measured and computed dune profiles for LB and LW tests are compared in Fig. 5 where the number of runs for LB and LW tests were 3 and 20, respectively. The crest lowering of the low dune was limited by the vertical wall with its crest elevation at 6 cm above SWL. The profile

lowering of the bare dune and the dune with the wide dowel zone is predicted fairly well except for the computed undulation in front of the vertical wall.

Fig. 6 compares the measured and computed values of q_o and q_{bs} for LB and LW tests. For LB test, the measured values of q_o and q_{bs} were large from the first run and the agreement is better than that for HB test in Fig. 4. For LW test, q_o is overpredicted by a factor of about 2 but the agreement for q_{bs} is good. It is difficult to predict both q_o and q_{bs} accurately because wave overtopping and overwash depend on the hydrodynamics and sediment dynamics in the wet and dry zone where the computed water depth is of the order of 1 cm or less.

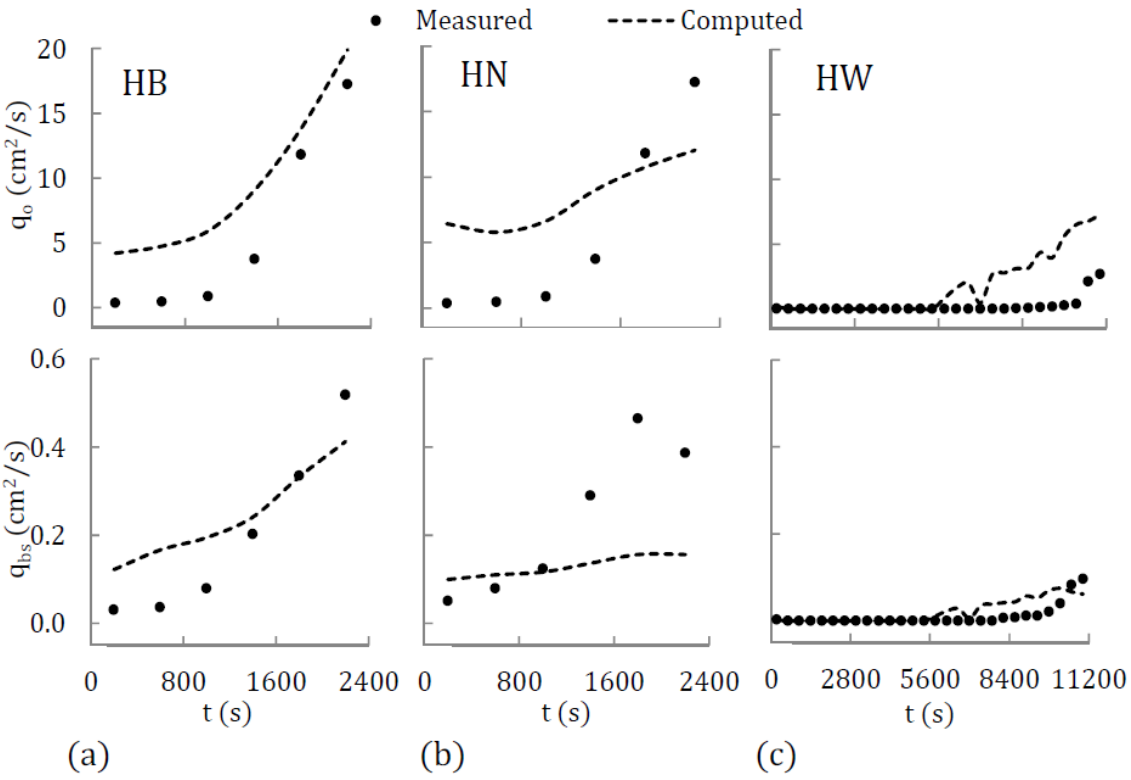

Figure 4. Measured and computed wave overtopping rate q_o and sand overwash rate q_{bs} for (a) HB, (b) HN and (c) HW tests.

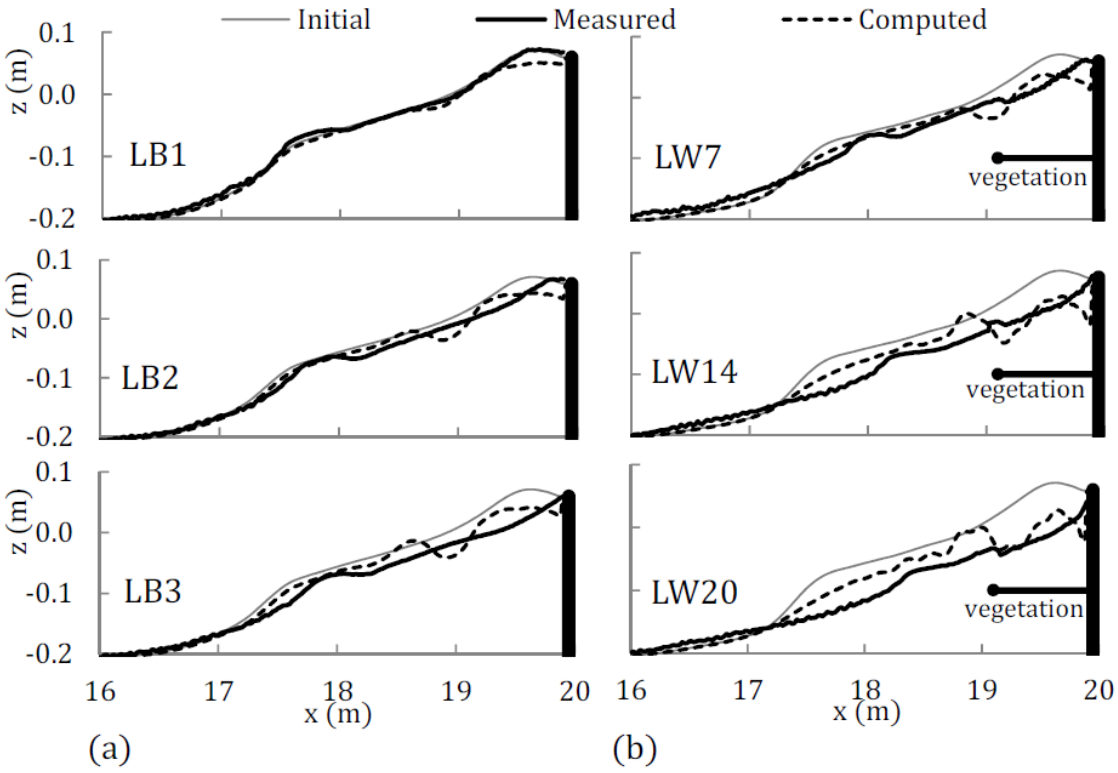

Figure 5. Measured and computed dune profiles at the end of three runs for (a) LB and (b) LW tests.

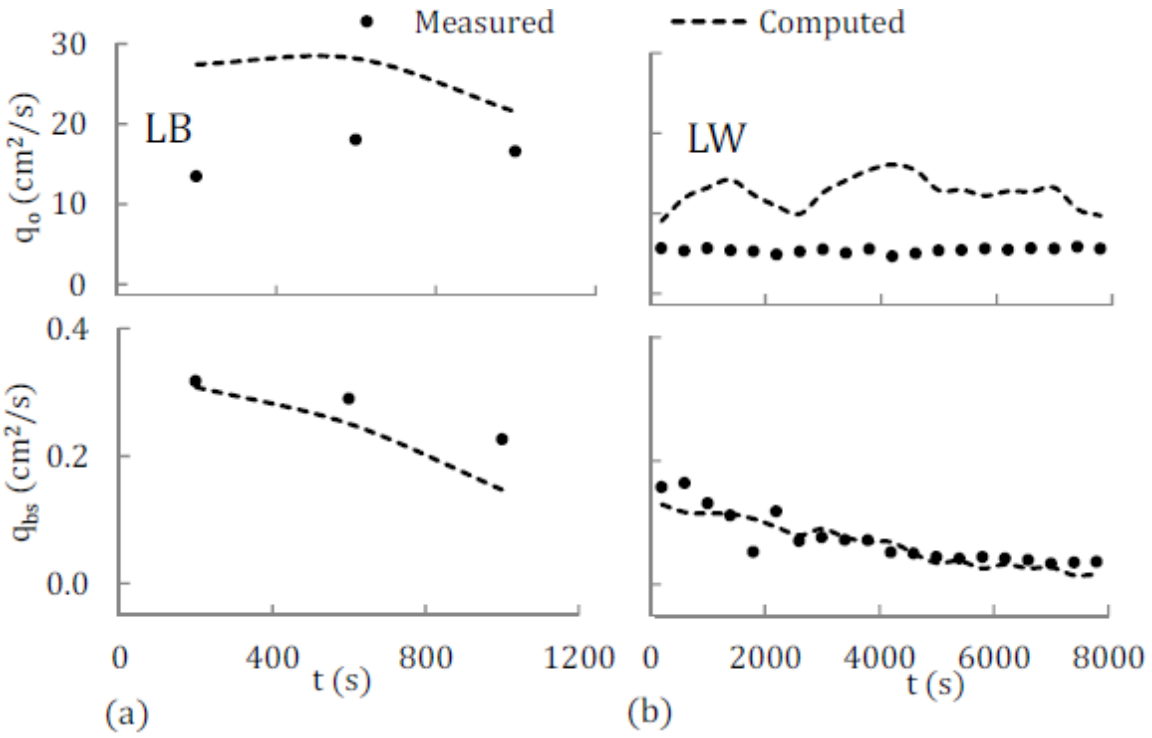

Figure 6. Measured and computed wave overtopping rate q_o and sand overwash rate q_{bs} for (a) LB and (b) LW tests.

4. Dowel Density Effect

The calibration of the drag coefficient in the range of $C_D = 1-2$ has indicated the increase of dune erosion with the decrease of C_D, especially for HW test when the wave overtopping rate q_o is zero or very small. The drag force τ_d in Eqs. (2) and (6) is proportional to the product of $(C_D bN)$ with $N = 1/S^2$ where the dowel diameter $b = 0.9$ cm and spacing $S = 4$ cm for HN, HW and LW tests. The drag force was not measured in the experiment and the dowel diameter cannot be changed for the existing dowels. The dowel spacing for HW test was changed to $S = 6$ cm (sparse) and $S = 4.24$ cm (dense) where the dowel density N was varied by a factor of 2 between the sparse (S) and dense (D) dowel tests as listed in Table 1. This dowel density difference is the same as the range of the drag coefficient calibration. The dowel height $d = 10$ cm and burial depth $d_b = 20$ cm for HW test were kept the same for these deep (D) burial tests of no toppling. The number of runs for SD and DD tests were 8 and 29, respectively, for the dune crest lowering to the level of the vertical wall crest. The sparse dowels for SD test were not effective in reducing dune erosion and overwash. The difference between DD and HW tests was small because of the small (about 10%) difference of their N values in Table 1. The limited data suggest that the reduction of dune erosion and overwash by the dowels may be negligible if the normalized dowel spacing (S/b) exceeds about 7.

Fig. 7 compares the measured and computed dune profiles at the end of three runs for SD and DD tests. The agreement for DD test is similar to that for HW test in Fig. 3 probably because $C_D = 1.9$ has been calibrated for the dense dowels. The dune scarping and crest lowering for SD

Table 1. Summary of Dowel Density and Toppling Tests

Test	$\frac{S}{b}$	N (m^{-2})	d (m)	d_b (m)	Number of Runs
HW	4.44	625	0.10	0.20	28
SD	6.67	278	0.10	0.20	8
DD	4.71	556	0.10	0.20	29
DF	4.71	556	0.05*	0.10*	9
DS	4.71	556	0.10*	0.05*	6

*Initial dowel height d and burial depth d_b for dowel toppling DF and DS tests.

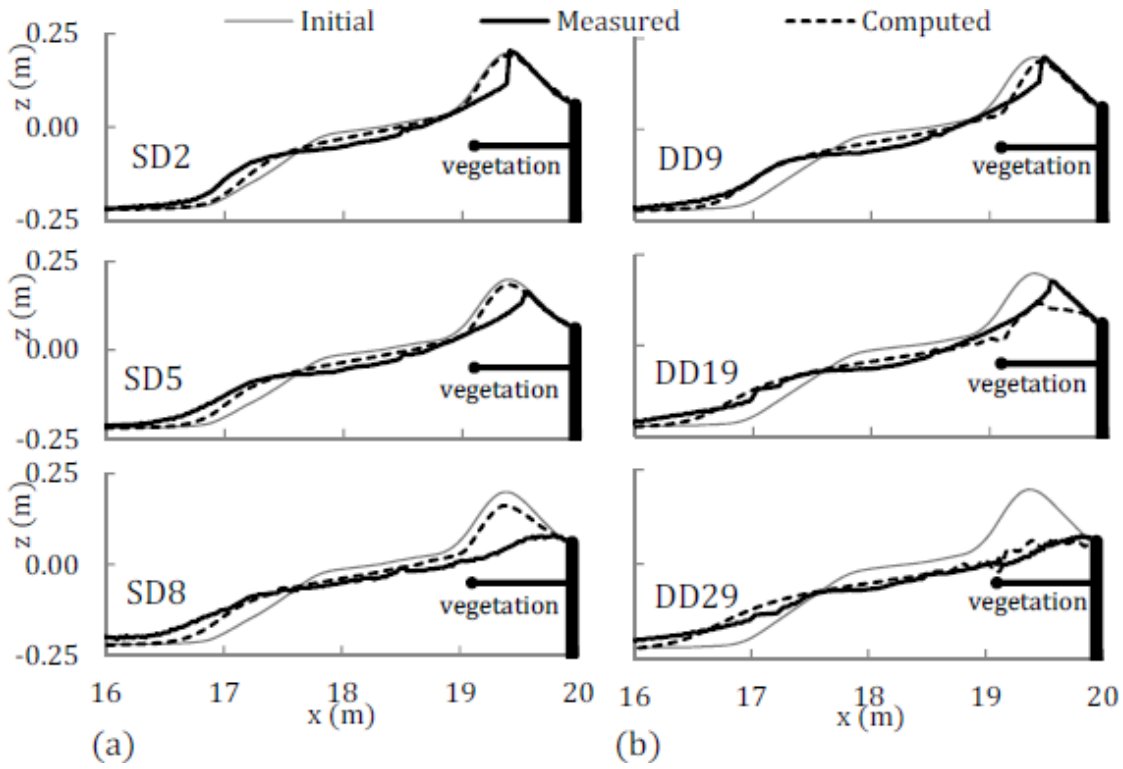

Figure 7. Measured and computed dune profiles at the end of three runs for (a) SD and (b) DD tests for sparse (S) and dense (D) spacing of dowels buried deep (D).

test is underpredicted and the value of C_D needs to be reduced to increase the dune crest lowering for the sparse dowels. This implies that C_D may depend on the dowel density N. The measured dune profile evolutions for SD and DD tests appear similar apart from the dowel density difference and evolution rate (run number) difference.

The measured and computed temporal variations of q_o and q_{bs} are compared in Fig. 8. The measured wave overtopping rate q_o and overwash rate q_{bs} were zero or very small until the dune crest was lowered sufficiently. The measured rapid increase of q_o and q_{bs} for SD test is underpredicted because of the underpredicted dune crest lowering in Fig. 7. The initiation of wave overtopping and overwash is predicted to occur too early for DD test. The numerical model is not refined enough to predict both the dune crest lowering and wave overtopping initiation accurately.

5. Dowel Toppling Effect

The preceding tests were limited to the dowel height $d = 10$ cm and burial depth $d_b = 20$ cm throughout the tests. The dowel top was emergent above uprushing and downrushing water and no dowel toppling occurred. To allow the occurrence of dowel submergence and toppling, the 30-cm long dowel was cut in half to create two 15-cm long dowels. These short dowels were placed in the same pattern as the dense (D) dowels for DD test with the deep (D) burial depth $d_b = 20$ cm for no toppling. Two toppling tests were conducted for the finite (F) and shallow (S) burial depths $d_b =$ 10 and 5 cm as listed in Table 1. The dowel toppling increased dune erosion and the number of runs were 9 and 6 for DF and DS tests, respectively. For DF and DS tests with

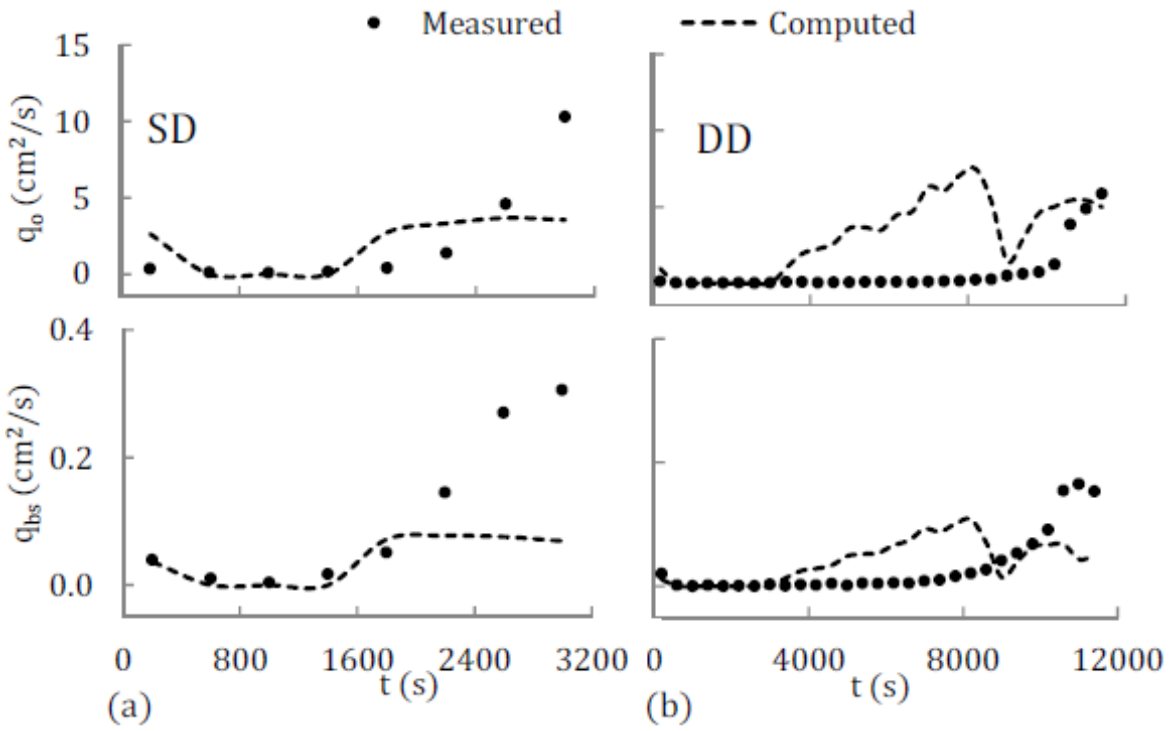

Figure 8. Measured and computed wave overtopping rate q_o and sand overwash rate q_{bs} for (a) SD and (b) DD tests.

$(d+d_b)=15$ cm, the elevations of the top and bottom of each vertical dowel were kept constant during each test. The dowel height and burial depth changed as the bottom elevation $z_b(t,x)$ at given x changed with time t during each test. The erosion depth $d_e(t,x)$ below the initial bottom elevation $z_b(t=0,x)$ is defined as $d_e(t,x)=\left[z_b(t=0,x)-z_b(t,x)\right]$ where $d_e<0$ for deposition. The drag force τ_d given by Eqs. (2) and (6) is computed using the actual height $(d+d_e)$ in place of the initial height d. The actual burial depth (d_b-d_e) normalized by the dowel diameter $b=0.9$ cm is used to develop a simple toppling criterion.

For the dense dowel placement of DF and DS tests, 26 dowels were place alongshore at 19 cross-shore locations. During the 400-s run, some dowels were toppled by the wave force and floated in uprushing and downrushing water. After each run, the placement location of each toppled dowel was recorded. The toppled dowels were removed before the next run. The observed dowel toppling was not uniform alongshore, whereas the numerical model assumes alongshore uniformity. Dowel toppling at each of the 19 cross-shore locations is regarded to have occurred when at least 14 out of the 26 alongshore dowels were toppled. The run number corresponding to this toppling definition is identified at each of the 19 cross-shore locations. The values of the burial depth (d_b-d_e) at given x before and after the toppling run are obtained where the bottom elevation z_b was measured at time $t=0$ and after each run. Fig. 9 shows the values of $(d_b-d_e)/b$ before and after the toppling run at given x. The difference between the no toppling and toppling values is the increment of the erosion depth d_e normalized by b during the toppling run. The increase of the erosion depth during the toppling run was large on the foreslope of the dune because the overturned dowels lifted some of the surrounding sand. No

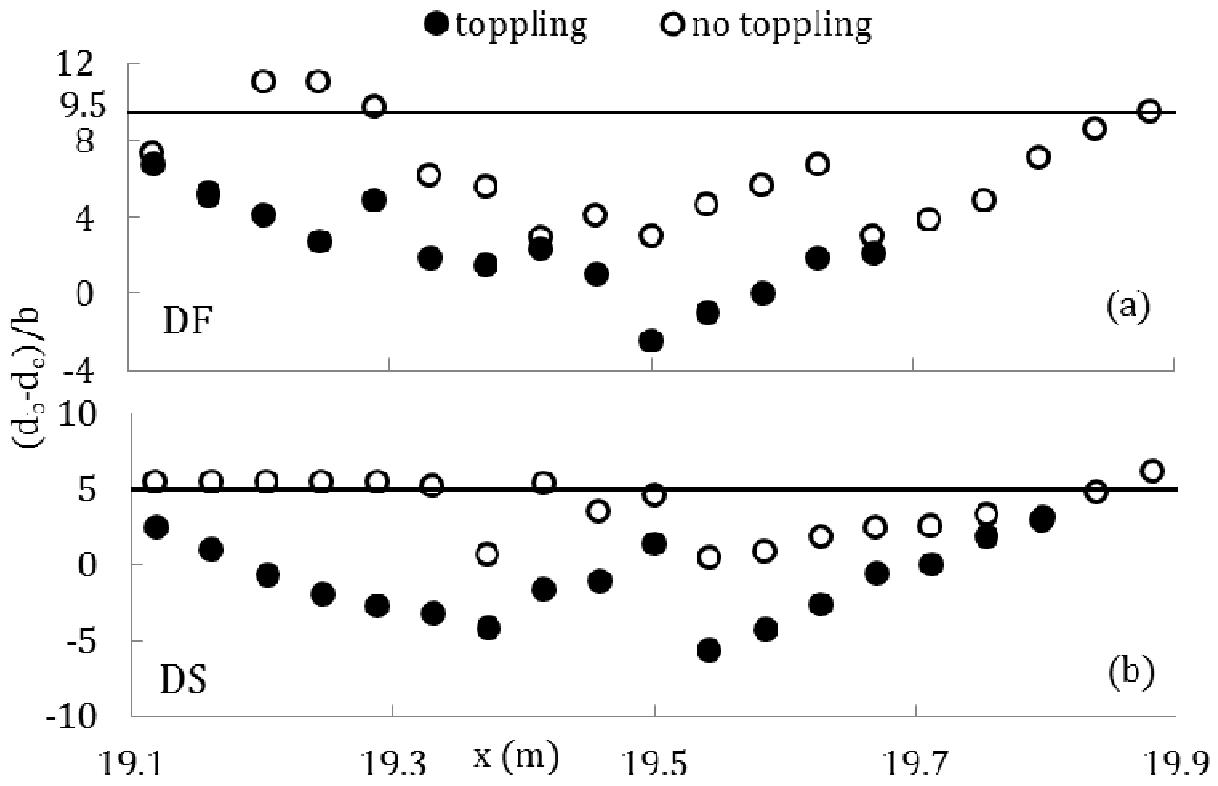

Figure 9. Calibrated toppling coefficient C_u based on toppling of dowels on foreslope of dune for (a) DF and (b) DS tests for finite (F) and shallow (S) burial depths of dense (D) dowels.

toppling occurred at the 5 and 2 cross-shore locations next to the vertical wall at $x = 19.9$ m for DF and DS tests, respectively. These locations correspond to the locations without toppling values in Fig. 9.

The toppling effect is included in CSHORE using the following criterion:

$$(d_b - d_e)/b < C_u \quad \text{for toppling} \tag{10}$$

where C_u = dimensionless toppling coefficient calibrated as $C_u = 9.5$ for DF test and $C_u = 5$ for DS test. This simple criterion does not account for the initial dowel height d which was different for the two tests. The adequate reproduction of the landward progression of dowel toppling on the foreslope of the dune is found to be necessary for the prediction of dune erosion and overwash. The calibrated C_u for each test is plotted in Fig. 9 to show that the calibrated C_u represents the occurrence of dowel toppling on the foreslope of the dune. Fig. 10 shows the measured and computed landward progression of dowel toppling where the toppling time t_u in the middle of the toppling run at given x is plotted at each of the 19 cross-shore dowel locations. The upper bound of t_u is the test duration and t_u = 3,600 s (2,400 s) for DF (DS) test at the cross-shore locations of no toppling. The calibration of C_u for each test has been performed to reproduce the measured toppling progression in Fig. 10. The agreement for the toppling tests has become as good as that for the other tests after the calibration of C_u as shown in the following.

The measured and computed cross-shore variations of $\overline{\eta}, \sigma_\eta, \overline{U}, \sigma_U$ and P_w have been compared for each run of SD, DD, DF and DS tests in order to confirm that the hydrodynamic variables are predicted within errors of about 20%. The comparisons for DF1 (first) and DF9 (last) runs are shown in Fig. 11 as examples in the same way as in Fig. 2. It should be noted that

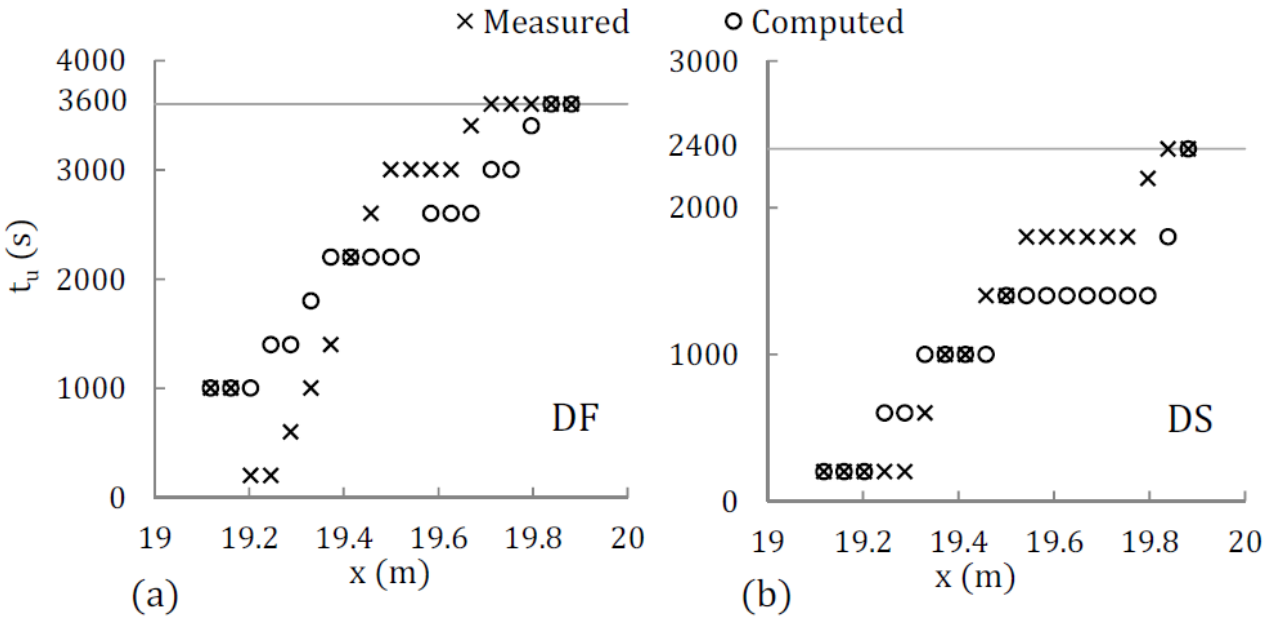

Figure 10. Measured and computed landward (increasing x) progression of toppling time t_u in the middle of toppling run for (a) DF and (Ob) DS tests.

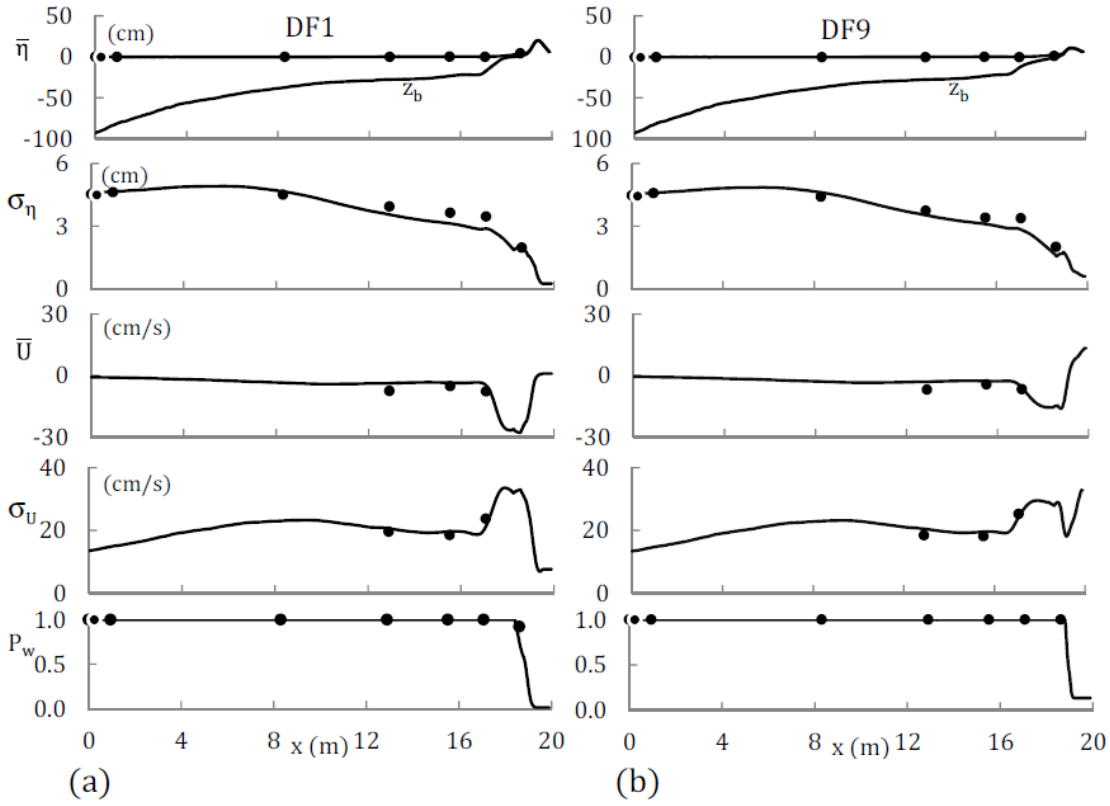

Figure 11. Measured (circles) and computed (solid lines) mean and standard deviation of η and U together with wet probability P_w for (a) DF1 and (b) DF9 runs.

no measurement was made of the depth and velocity in the dowel zone on the dune. Such measurements would allow more direct calibration of the drag coefficient C_D and the toppling coefficient C_u used in the expanded numerical model.

Fig. 12 compares the measured and computed dune profiles at the end of three runs for DF and DS tests. The dune scarping and crest lowering are underpredicted for both tests. The landward progression of dowel toppling in Fig. 10 and the dune crest lowering in Fig. 12 are correlated positively. Both occurred faster for DS test than DF test. The measured dune profile evolutions for DD, DF and DS tests in Figs. 7 and 12 appear similar apart from the evolution rates represented by the run numbers. The dune profile evolution is influenced by the wave overtopping rate q_o and overwash rate q_{bs}.

Fig. 13 compares the measured and computed temporal variations of q_o and q_{bs} for DF and DS tests. The agreement for these toppling tests is better than that for DD test in Fig. 8. The dune crest lowering accelerated when q_o and q_{bs} increased rapidly. Figs. 10, 12 and 13 indicate that the effectiveness of the dowels in reducing dune erosion and overwash arises mostly from the reduction of wave uprush and overtopping by the dowels on the foreslope of the dune. The dowel effectiveness diminishes after the dowel toppling on the foreslope.

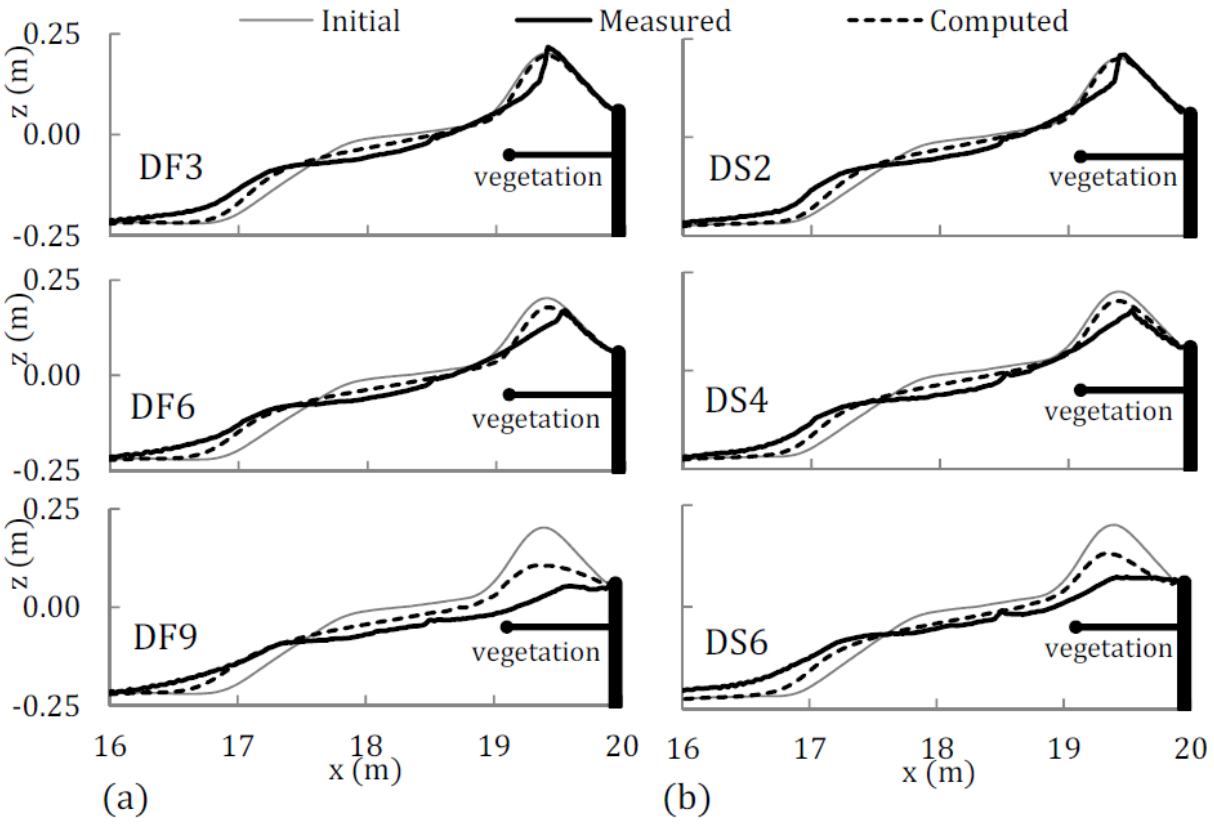

Figure 12. Measured and computed dune profiles at the end of three runs for (a) DF and (b) DS tests.

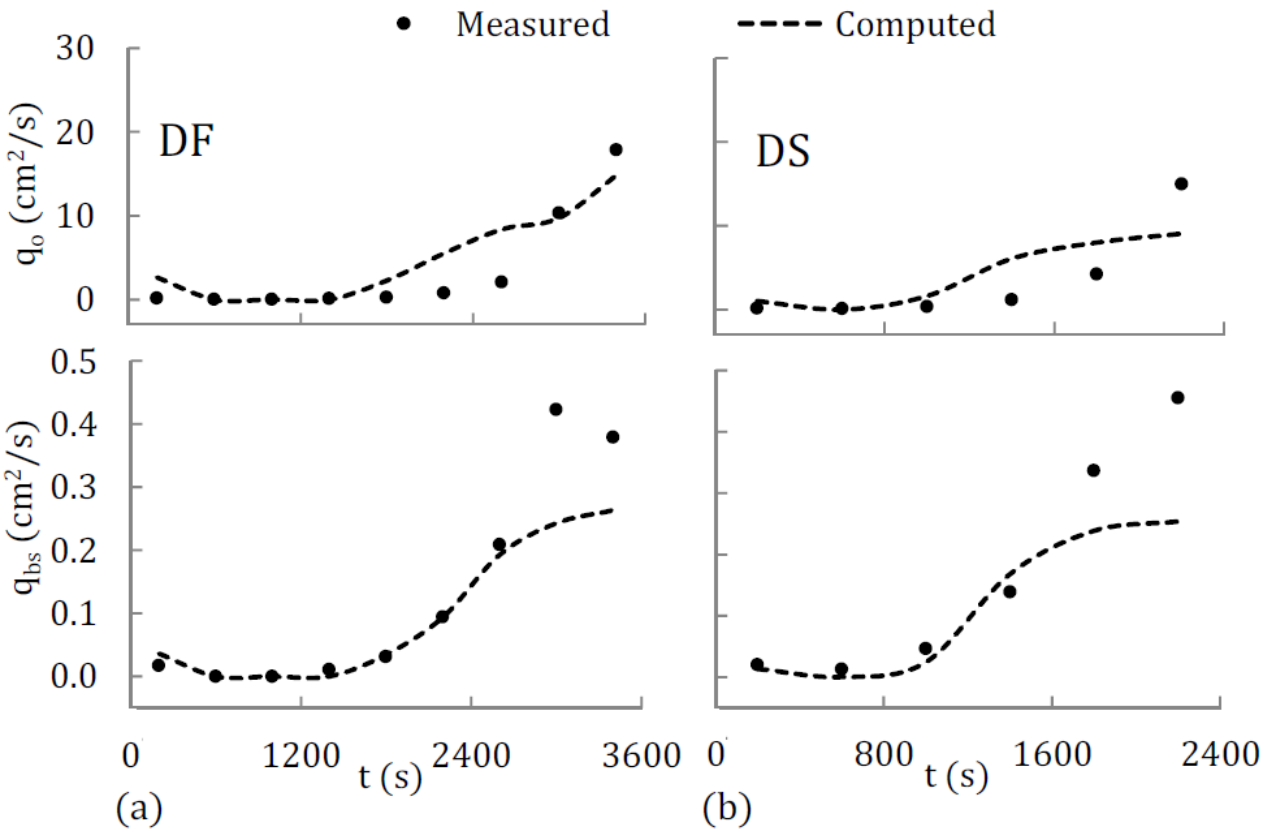

Figure 13. Measured and computed wave overtopping rate q_o and sand overwash rate q_{bs} for (a) DF and (b) DS tests.

6. Conclusions

The cross-shore numerical model CSHORE is expanded to include the drag force acting on dowels and the resulting dissipation of wave energy. The hydrodynamic variables modified by the dowels are used to predict the bed load and suspended sediment transport rates using the formulas developed for the case of no dowels. The buried parts of the dowels are not considered in this model. The expanded model was compared with 3 high dune and 2 low dune tests by Gralher et al. (2012) . The cross-shore variations of the mean and standard deviation of the free surface elevation and cross-shore velocity were predicted within errors of about 20%. The profile evolutions of the dunes with and without the dowels were predicted within a factor of about 2. The ineffectiveness of the narrow dowel zone on the steep backslope of the high dune was reproduced by the model. The effectiveness of the wide dowel zone covering the high and low dunes in reducing the wave overtopping and sand overwash rates was also reproduced but these rates were difficult to predict accurately in spite of the use of the drag coefficient $C_D = 1.9$ calibrated for the condition of no or little overtopping.

Two high dune tests were conducted to examine the effect of the spacing S and density $N = 1/S^2$ of the dowels of diameter b covering the entire dune. The effectiveness of the dowels in reducing dune erosion and overwash diminished when the ratio S/b became larger than about 7. The numerical model with the calibrated drag coefficient predicted this density effect. Additional two tests were conducted to examine the toppling effect of the dowels covering the high dune. An empirical toppling coefficient was introduced in the model and calibrated to mimic the observed landward progression of dowel toppling for each of the two tests. The

toppling of the dowels on the foreslope of the high dune diminished the effectiveness of the dowels in reducing dune erosion and overwash because the dowels on the foreslope reduced wave uprush and overtopping. The toppling coefficient will need to be calibrated for real woody plants to apply the expanded numerical model to prototype wooded dunes. Field data will be required to improve the dowel model.

7. References

Edge, B.L., Ewing, L., Dean, R.G., Kaihatu, J.M., Overton, M., Rogers, S.M., and Work, P. (2010). "Immediate impacts of Hurricane Ike on Texas Coast." Proc. 32nd Coastal Engineering Conf., Management 14, 1-16, http://journals.tdl.org/ICCE .

Figlus, J., Kobayashi, N. and Gralher, C. (2012). "Onshore migration of emerged ridge and ponded runnel." *J. Waterway, Port, Coastal, Ocean Eng.*, 138(5), 331-338.

Figlus, J., Kobayashi, N., Gralher, C., and Iranzo, V. (2011). "Wave overtopping and overwawsh of dunes." *J. Waterway, Port, Coastal, Ocean Eng.*, 137(1), 26-33.

Gralher, C., Kobayashi, N., and Do, K. (2012). "Wave overwash of vegetated dunes." *Proc. 33rd Coastal Engineering Conf.*, Sediments 34, 1-7, http://journals.tdl.org/ICCE.

Horstman, E., Dohmen-Janssen, M., Narra, P., van der Berg, N., Siemerink, M., Balke, T., Bouma, T., and Hulscher, S. (2012). "Wave attenuation in mangrove forests: Field data obtained in Trang, Tahiland." Proc. 33rd Coastal Enginheering Conf., Waves 40, 1-15, http://journals.tdl.org/ICCE .

Kobayashi, N., Farhadzadeh, A., Melby, J.A., Johnson, B.D., and Gravens, M. (2010). "Wave overtopping of levees and overwash of dunes." *J. Coastal Research*, 26(5), 888-900.

Kobayashi, N., Gralher, C., and Do, K. (2013). “Effects of woody plants on dune erosion and overwash.” *J. Waterway, Port, Coastal, Ocean Eng.*, 139(6), 466-472.

Kobayashi, N., and Jung, H. (2012). “Beach erosion and recovery.” *J. Waterway, Port, Coastal, Ocean Eng.*, 138(6), 473-483.

Matsutomi, H., Yamaguchi, E., Naoe, K., and Harada, K. (2012). “Damage to reinforced concrete buildings and coastal trees due to the 2011 off the Pacific coast of Tohoku Earthquake Tsunemi.” Proc. 33rd Coastal Engineering Conf., Management 51, 1-13, http://journals.tdl.org/ICCE .

Tørum, A. (1989). “Wave forces on pile in surface zone.” *J. Waterway, Port, Coastal, Ocean Eng.,* 115(4), 547-565.